Analytica Chimica Acta 670 (2010) 57–62

Contents lists available at ScienceDirect

Analytica Chimica Acta

journal homepage: www.elsevier.com/locate/aca

# Electrochemical biosensor for the detection of $H_2O_2$ from living cancer cells based on ZnO nanosheets

Qi Rui [a], Kikuo Komori [b], Yang Tian [a,c,*], Haiqing Liu [a], Yongping Luo [a], Yasuyuki Sakai [b]

[a] Department of Chemistry, Tongji University, Siping Road 1239, Shanghai 200092, PR China
[b] Institute of Industrial Sciences, University of Tokyo, 4-6-1 Komaba, Meguro-ku, Tokyo 153-8505, Japan
[c] State Key Laboratory of Chemo/Biosensing and Chemometrics, Hunan University, Changsha 410082, PR China

ARTICLE INFO

*Article history:*
Received 30 July 2009
Received in revised form 9 October 2009
Accepted 30 April 2010
Available online 7 May 2010

*Keywords:*
ZnO nanosheets
Cytochrome *c*
$H_2O_2$
Electrochemical biosensor
Living cells

ABSTRACT

In this work, direct electron transfer of cytochrome *c* (cyt. *c*)—a model for studying the electron transfer of enzymes is achieved at hexagonal ZnO nanosheets by one-step electrodeposition. UV–vis spectra and electrochemical data demonstrate that such ZnO nanosheets can supply a bio-compatible surface to keep the bioactivity of cyt. *c*. The redox formal potential ($E^{0\prime}$) of cyt. *c* is estimated to be $338.2 \pm 4.3$ mV (vs. Ag|AgCl) at the nanostructured ZnO surface. This value is much more positive than those of enzymes previously obtained at other metal oxides and zeolite surfaces. Experiment data show, under the optimized potential of 0.0 V (vs. Ag|AgCl), the electrochemical determination of $H_2O_2$ is free from not only anodic interferences like ascorbic acid (AA) and dopamine (DA), but also a cathodic interference—$O_2$. Such an excellent selectivity enable the present $H_2O_2$ biosensor determine the extracellular $H_2O_2$ released from living human hepatoma cells.



## 1. Introduction

Since determination of $H_2O_2$ is of practical importance in biological, clinical, environmental, industrial, and many other fields, a number of strategies, such as titrimetry, spectrophotometry, chemiluminescence, and electrochemical methods have been developed to detect $H_2O_2$ [1–4]. Electrochemical approaches have been gained increasing attentions for the determination of $H_2O_2$ in vivo and in vitro because of the high selectivity, sensitivity, and capability. For rapid diagnostics of $H_2O_2$, the third-generation biosensors have been developed, which are based on the direct electron transfer (DET) of enzymes with a superior selectivity and sensitivity. Thus, a burst of research activities has been paid on modification of electrodes or proteins for creating accessible electron transfer interfaces, subsequently constructing the third-generation biosensors [5,6]. Cyt. *c* is an excellent model for studying the electron transfer of typical metalloproteins from a structure point of view. In the past couple of decades, numerous applications of chemically or non-chemically modified methods to direct electron transfer of cyt. *c* have been exploited [7–12]. Recently, metal nanoparticles have widely employed for the direct electron transfer of cyt. *c*. Natan and co-workers have realized the reversible electrochemistry of cyt. *c* and suggest that the size of gold nanoparticles (AuNPs) plays an important role in protein electrochemistry [13–15]. Our group has systematically investigated the DET of cyt. *c* at different shapes of AuNPs and has constructed the third-generation biosensor for $H_2O_2$ [16].

It is well-known that a $H_2O_2$ sensor for using in biological system must overcome the great interferences from other coexisting species, in particular AA and the changes in the endogenous levels of $O_2$ that are associated with the formation of $H_2O_2$ under pathophysiological conditions [17,18]. Up to now, most of the $H_2O_2$ biosensors based on DET of enzymes mentioned above are easy to avoid the anodic interferences like AA, DA, because the redox potentials of proteins at semiconductors surfaces are almost observed at negative potentials, as a consequence the potentials of those $H_2O_2$ biosensors are usually operated at negative potentials [19–22]. However, the reductive potential of $O_2$ is commonly more positive than that of $H_2O_2$, thus it is very hard to detect $H_2O_2$ free from the interference of $O_2$ at those negative potentials, regardless that $O_2$ exists extensively in the biological system, and is associated with the formation of $H_2O_2$. Recently, the direct electron transfer of cyt. *c* has been realized at $WO_3$ nanomaterials at formal potentials of $-133.5 \pm 1.7$ mV [23], and on the basis of these experiments, $H_2O_2$ has been determined with high selectivity and wide linear range. However, few papers are concerned with the DET of cyt. *c* at ZnO nanostructures, although ZnO demonstrates a slightly lower conduction band edge and higher density of sub-

* Corresponding author at: Department of Chemistry, Tongji University, Siping Road 1239, Shanghai 200092, PR China. Tel.: +86 21 65987075; fax: +86 21 65982287.
*E-mail address:* yangtian@mail.tongji.edu.cn (Y. Tian).

0003-2670/$ – see front matter © 2010 Elsevier B.V. All rights reserved.
doi:10.1016/j.aca.2010.04.065

band gap states than $TiO_2$, resulting in significant conductivities and electrochemical activities [24,25].

In this work, the DET of cyt. *c* is first realized at hexagonal ZnO nanosheets with formal potential of $338.2 \pm 4.3$ mV vs. Ag|AgCl. Spectroscopic and electrochemical results demonstrated that cyt. *c* is stably adsorbed on the nanostructured ZnO film and processes its intrinsic enzymatic activity toward $H_2O_2$. A combination of direct electrochemistry of cyt. *c* at ZnO nanosheets and enzymatic catalytic activity of cyt. *c* toward $H_2O_2$ pave a way for constructing a third-generation biosensor for $H_2O_2$. Moreover, the relatively positive redox potential of cyt. *c* obtained at the present ZnO nanosheets is very benefit for cathodic detection of $H_2O_2$ with relatively high selectivity. Under the optimized potential of 0.0 V (vs. Ag|AgCl), the present $H_2O_2$ biosensor is easy to avoid not only the anodic interferences, such as UA, AA, and DA, but also cathodic interference—$O_2$. Therefore, such a biosensor shows predominance in determining extracellular $H_2O_2$ released from human hepatoma cell line Hep G2.

## 2. Experimental

### 2.1. Reagents

Horse heart cytochrome *c* (MW 13 000) was purchased from Sigma and used without further purification. Phobol 12-myristate 13-acetate (PMA) was obtained from Wako Pure Chemical Industries (Osaka, Japan). Human hepatoma cell line Hep G2 was obtained from Japanese Cancer Research Resources Bank (Tokyo, Japan). The cells were maintained in a culture medium consisting of Delbecco's modified minimum essential medium (DMEM; Wako Pure Chemicals, Japan) and subcultured every five days. Ascorbic acid was purchased from Sinopharm Chemical Reagent Co., Ltd. (China). Uric acid, 99% (Alfa Aesar) was used without further purification. Other reagents were of analytical grade and used as received. ITO-coated glass plates with a square resistance of $\sim 10\,\Omega\,cm^{-2}$ were purchased from Shenzhen Nanbo Display Technology Co. Ltd. (Shenzhen, China). All the solutions were prepared with Milli-Q water. Except the interference test of $O_2$ (under $O_2$ saturated solution), all the experiments were deaerated with high purity nitrogen before experiments. All electrochemical experiments were carried out at room temperature.

### 2.2. Apparatus

CHI 660 electrochemical work stations (CH Instruments) were employed in all electrochemical measurements which were carried out with a conventional two-compartment three-electrode electrochemical cell. The reference electrode was a KCl-saturated Ag|AgCl electrode, while the auxiliary electrode was a platinum wire. SEM images were taken by a Quanta 200 FEG (FEI Company). UV–vis absorption spectrum was collected by an Agilent 8453 UV–vis-near-infrared spectrophotometer (Agilent Instruments).

### 2.3. Preparation of cyt. c modified ZnO Film

ZnO nanosheets film was fabricated by electrodeposition (our previous work [26] for details). Prior to the modification of cyt. *c*, the ZnO film was annealed for 1 h at 773 K in oven. Then, immersing the ZnO film into PBS (pH 7.2) of cyt. *c* (0.2 mM) for about 0.5–3 h at 3 °C in refrigerator. Hereafter, cyt. *c* modified nano ZnO electrode will be referred as ZnO/cyt. *c*.

### 2.4. Real sample analysis

The Hep G2 cells were centrifuged to obtain a cell-packed pellet ($1.0–1.5 \times 10^5$ cells $cm^{-2}$) for the electrochemical experiments.

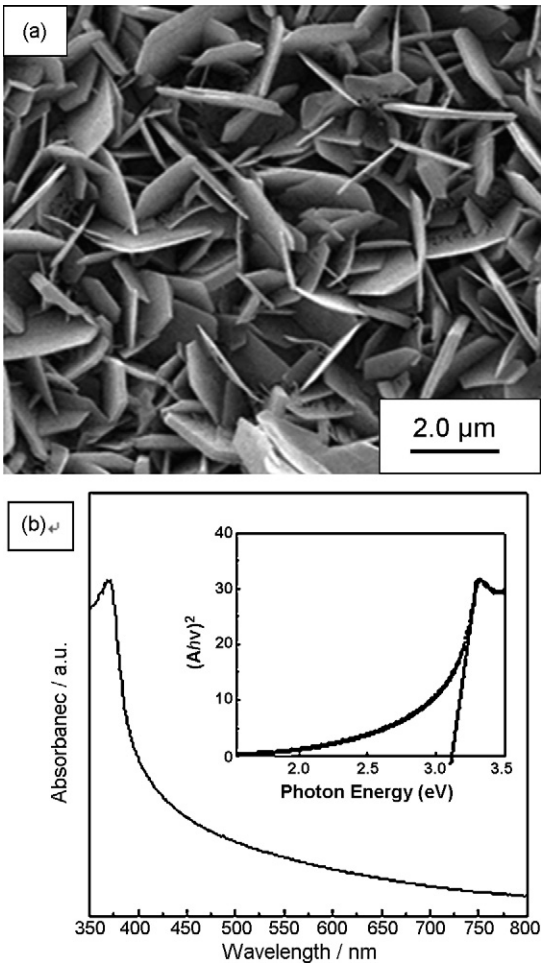


**Fig. 1.** (A) SEM images of electrodeposited ZnO nanosheets film. (B) UV–vis absorption spectrum of the ZnO nanosheets film. Inset: the spectrum for the ZnO nanosheets replotted as $(\alpha h\nu)^2$ vs. $h\nu$.

For the detection of extracellular $H_2O_2$, the geometric surface area of nanostructured ZnO film was fabricated to be 500 μm in width and 2 mm in length. Real sample measurements were performed in PBS containing (100 mM) glucose mounted onto a heated Faraday stage (37 °C). The device was viewed under a microscope. Under the microscope, the working electrode was located ~100 μm from the liver cells.

## 3. Results and discussion

### 3.1. Characterization of ZnO nanosheets film and cyt. c adsorbed onto the ZnO film

The electrodeposited ZnO nanosheets film was prepared as described in Section 2 and was characterized by scanning electron microscopy (SEM). As shown in Fig. 1, most of the ZnO nanosheets are rather regular hexagons, and the contrast on a whole sheet is homogenous. Many nanosheets have regular edges with an angle of 120°, which corresponds to the angles between the {0 1 − 1 0} planes of the wurzite ZnO crystal structure [27,28]. The ZnO nanosheets are typically 50–80 nm in thickness and several micrometers in dimension.

UV–vis absorption spectrum of the nanostructured ZnO film was shown in Fig. 1(B). For a direct bandgap semiconductor like ZnO, the

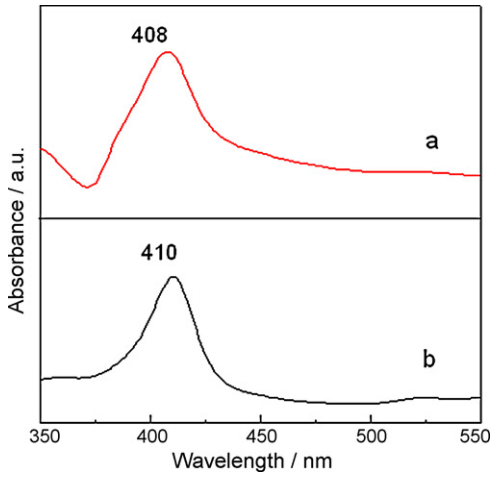


**Fig. 2.** UV–vis absorption spectra of (a) cyt. *c* adsorbed on the nanostructured ZnO film and (b) 0.2 mM cyt. *c* solution.

absorbance in the vicinity of the onset is given by:

$$\alpha = \frac{C(h\nu - E_g^{\text{bulk}})^{1/2}}{h\nu} \quad (1)$$

where $\alpha$ is the absorption coefficient, $C$ is a constant, $h\nu$ is the photon energy, and $E_g^{\text{bulk}}$ is the bulk bandgap [28]. The inset in Fig. 2 demonstrates the absorbance spectrum for the ZnO nanosheets replotted according to Eq. (1). The intercept at *x*-axis yields a bandgap of 3.11 eV. The UV–vis absorption spectrum shows considerable absorption below the band gap. This observation is possible that the impurities in the ZnO nanostructures, size and shape distribution of the ZnO nanoparticles, and the surface defects may broaden the absorption edge of the present ZnO nanosheets [29,30].

For further investigation on the electrochemistry and electrocatalytic activity of cyt. *c* confined on the nanostructured ZnO surface, it is desirable to clarify whether cyt. *c* is denatured after immobilized on the ZnO nanostructures. The Soret band of heme protein is usually an indicator of the microenvironment where heme center locates. The peak will be diminished if the protein is denatured [31,32]. Fig. 2 depicts UV–vis absorption spectra of cyt. *c* confined on the optical transparent ZnO nanosheets surface (a) and 0.2 mM cyt. *c* in solution (b). The band for cyt. *c* adsorbed on the nanostructured ZnO film is located at 408 nm, just a 2-nm blue shift compared with that of native cyt. *c* solution (410 nm). This spectrum suggests that there is no obvious denaturation for cyt. *c* adsorbed on the ZnO nanosheets.

### 3.2. Direct electrochemistry of cyt. c at the ZnO nanosheets film

Fig. 3(A) shows typical cyclic voltammograms (CVs) of the nanostructured ZnO film (a), and ZnO/cyt. *c* electrode (b) in 25 mM PBS (pH 7.2) containing no protein. Only charge current was observed at the ZnO nanosheets surface (a), while a pair of redox peaks of cyt. *c* with a peak width at half peak height ($\Delta E_{p,1/2}$) of $\Delta E_p = 102.4 \pm 2.1$ mV (average times $n = 4$) was observed. The formal potential ($E^{0\prime} = (E_{p,a} + E_{p,c})/2$) of cyt. *c* confined on ZnO film is estimated to be $338.2 \pm 4.3$ mV ($n = 4$) vs. Ag|AgCl, which is much more positive than those obtained at $TiO_2$, $WO_3$, $SnO_2$, $SiO_2$, $Nb_2O_5$, and NaY zeolite surfaces [33–38]. Both the anodic and the cathodic peak currents ($I_p^a$ and $I_p^c$) vary linearly with potential scan rate ($\nu$) (Fig. 3(B)), which is the characteristic of thin-layer electrochemistry [33]. In addition, the CVs remained essentially unchanged on consecutive potential scanning up to 1000 cycles at sweep rate of 20 mV $s^{-1}$, indicating that cyt. *c* was stably immobilized on the nanostructured ZnO film. According to Laviron's procedure, the relevant kinetic parameters of the electrode reaction, i.e. the rate constant of the electrochemical process ($k_s$) and cathodic transfer coefficients ($\alpha_c$), were estimated: $k_s = 4.62 \pm 0.07\ s^{-1}$, $\alpha_c = 0.48 \pm 0.03$ at the nanostructured ZnO surface. It reveals that the DET of cyt. *c* is strikingly enhanced at the nanostructured ZnO surface. ZnO/cyt. *c* nanocomposites show quasi-reversible electrochemistry with formal potential of 338.2 mV (vs. Ag|AgCl) and $k_s$ value of 4.62 $s^{-1}$. $k_s$ of electron transfer for cyt. *c* at the ZnO nanosheets is greater than those obtained at $SnO_2$, $SiO_2$, $Nb_2O_5$, and NaY zeolite electrodes, although which is smaller than those at $TiO_2$ and $WO_3$ surfaces [33–38]. By integration of the anodic peaks in CV, the charges and thus the average surface concentration of electroactive species could be calculated. The average surface concentration of electroactive cyt. *c* adsorbed on the nanostructured ZnO film was estimated to be $(7.42 \pm 0.21) \times 10^{-12}$ mol $cm^{-2}$. Taking account of the size (2.6 nm × 3.2 nm × 3.0 nm) [39] of cyt. *c* molecule, cyt. *c* molecules may be adsorbed on the ZnO nanosheets in a monolayer.

The adsorbed behavior of cyt. *c* was also confirmed by electrochemical impedance spectroscopy (EIS) (Supplementary material, Fig. S1). The charge transfer resistance ($R_{ct}$) of $Fe(CN)_6^{3-/4-}$ redox couple is about 60 Ω at ZnO nanosheets film, but it increases to 18.4 kΩ after cyt. *c* was immobilized on ZnO nanosheets. These data suggested that cyt. *c* adsorbed onto the nanostructured ZnO surface might inhibit the electrochemical communication between the

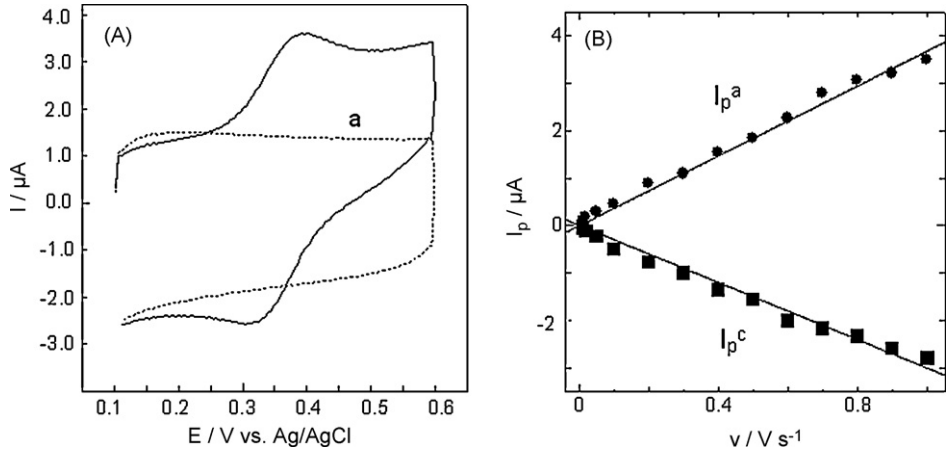


**Fig. 3.** (A) CVs obtained at (a) bare ZnO nanodisks film and (b) ZnO/cyt. *c* film in 25 mM PBS (pH 7.2). Potential scan rate: 100 mV $s^{-1}$. (B) Relationship between anodic and cathodic peak currents of ZnO/cyt. *c* film and scan rate.

electron transfer indicator—$Fe(CN)_6^{3-/4-}$ and the nanostructured ZnO electrode, resulting in the great increase of $R_{ct}$ of $Fe(CN)_6^{3-/4-}$ redox couple.

### 3.3. Analytical performance of the $H_2O_2$ biosensor

Cyt. *c* almost processes the enzymatic activity after immobilized on the ZnO nanosheets surface, which also facilitate the electron transfer of cyt. *c* itself. The interaction of $H_2O_2$ and cyt. *c* was studied using cyclic voltammetry. CVs of ZnO/cyt. *c* electrode in the absence (curve a), in the presence of $O_2$ (curve b) and in the presence of $H_2O_2$ (curve c) were obtained (Supplementary material, Fig. S2). CV of ZnO/cyt. *c* has almost no change in the presence of $O_2$, however the addition of $H_2O_2$ to 25 mM PBS (pH 7.2) obviously increases the cathodic currents of ZnO/cyt. *c* electrode, indicating the good electrocatalytical activity of the cyt. *c* confined on ZnO nanosheets for the reduction of $H_2O_2$, free from the interference of $O_2$. These results formed a strong basis for constructing the third-generation biosensor of $H_2O_2$ because the heme has been well documented as the active site for the catalysis to the reduction of $H_2O_2$.

The sensitivity of electrochemical biosensors is strongly dependent on the applied potential. The present $H_2O_2$ biosensor is no exception. As depicted in Fig. 4(A), the cathodic current intensity of $H_2O_2$ increased with the negative shift of the operating potentials. This sensitivity-potential profile gives the experimental basis for choosing the suitable operating potential for the measurement of $H_2O_2$. On the other hand, the selectivity of electrochemical biosensors is also potential-dependent. As well-known, the coexisting biological compounds, such as AA, DA, and $O_2$ may result in difficulties for electrochemical determinations of $H_2O_2$. Fig. 4(B) demonstrates four kinds of potential interferences under different applied potentials. Similar to the $H_2O_2$ biosensors previously reported, at the negative potentials, e.g., −0.1 and −0.05 V, the present $H_2O_2$ biosensor is free from the anodic interferences like AA, DA, $NO_2^-$, but 13.9 and 9.8% cathodic response currents of 0.2 mM $O_2$ were observed relative to 0.1 mM $H_2O_2$. At the positive potentials, e.g., +0.05 and +0.1 V, 4.0 and 6.7% anodic currents of 0.1 mM AA were obtained relative to 0.1 mM $H_2O_2$. Fortunately, at the applied potential of 0.0 V, both the anodic and the cathodic potential interferences were negligible. We also tried UA, mandelic acid, $NO_3^-$, and $SO_3^{2-}$ as interferential reagent. Likewise, the interferences were negligible (data not show). Therefore, for fulfill both the selectivity and the sensitivity of the present biosensor, 0.0 V (vs. Ag|AgCl) was selected as the optimized potential.

At the applied potential of 0.0 V (vs. Ag|AgCl), amperometric response of ZnO/cyt. *c* has been measured during the increase of $H_2O_2$ concentration and the corresponding current–time response is shown in Fig. 5. The solution was stirred with a magnetic stirrer at 200 rpm to make sure that the solution is mixed uniformly. Well-defined steady-state current response was obtained in 4 s at this applied potential, and the currents increased stepwise with additions of $H_2O_2$. The sensitivity of the present $H_2O_2$ biosensor is $2.0 \pm 0.1\ \mu A\ cm^{-2}\ mM^{-1}$. The calibration curve is depicted in the inset of Fig. 5. For the comparison, the control experiment was also carried out. No obvious current was observed at bare ZnO nanosheets film at 0.0 V with the addition of $H_2O_2$ (data not shown). In contrast with other $H_2O_2$ biosensors reported so far (Table 1) [40–42], besides higher selectivity, ZnO/cyt. *c* electrode shows wider linear detection range, lower detection limit, and shorter response time.

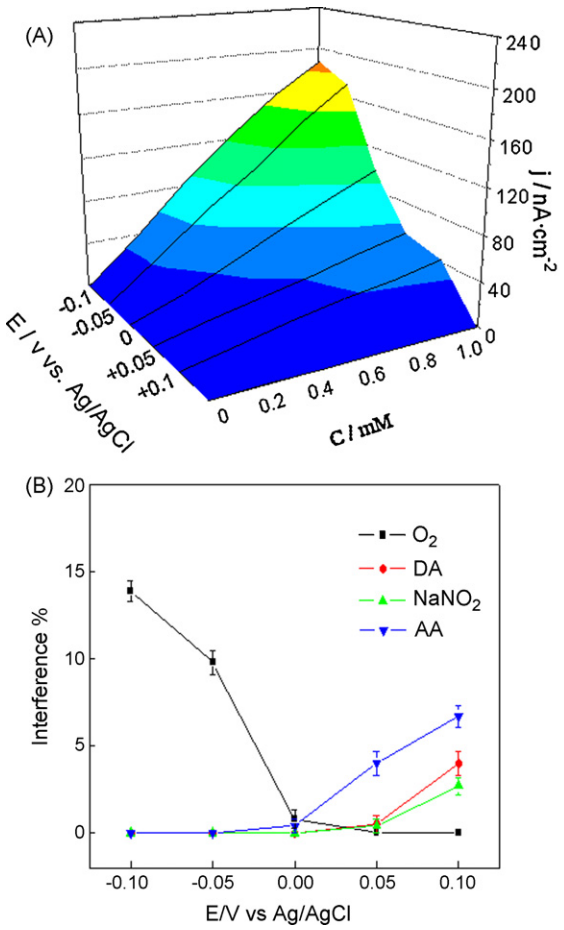


**Fig. 4.** (A) Calibration curves of the $H_2O_2$ biosensor obtained at different applied potentials: −0.1, −0.05, 0.0, 0.05, 0.1 V vs. Ag/AgCl. (B) The selectivity profile obtained at different applied potentials: −0.1, −0.05, 0.0, 0.05, 0.1 V vs. Ag/AgCl.

For the stability test, response current for $H_2O_2$ was recorded 2 times daily and the current response was found to be constant for at least 1 month, which holds relatively longer stability than that obtained at other $H_2O_2$ biosensors. In addition, we have found that the deviation of the current responses of over 5 sensors prepared with the same method did not exceed 4.7%.

### 3.4. Detection of extracelluar $H_2O_2$ released from human hepatoma cells

Fig. 6 demonstrates amperometric responses obtained at (a) ZnO nanosheets film and (b) ZnO/cyt. *c* electrode located near the human hepatoma cells Hep G2 in 25 mM PBS (pH 7.2) containing 100 mM glucose at the applied potential of 0.0 V vs. Ag|AgCl after the injection of (A) 3 mM phobol 12-myristate 13-acetate (PMA)

**Table 1**
Analytical properties of $H_2O_2$ biosensors based on ZnO-protein nanocomposites.

| Nanocomposites | Applied potential (mV vs. SCE) | Detection limit (μM) | Linear range (μM) | Reference |
|---|---|---|---|---|
| Cyt. c–ZnO nanosheets | −45 (0 mV vs. Ag\|AgCl) | 0.8 | 1–1000 | The present work |
| HRP–Chit–ZnO nanoflowers | −200 | 2 | 10–1800 | [35] |
| Mb-nanoporous ZnO films | ~−300 | 2 | 4.8–200 | [36] |
| Nafion/HRP/C-ZnO | ~−400 | 0.2 | 10–400 | [37] |

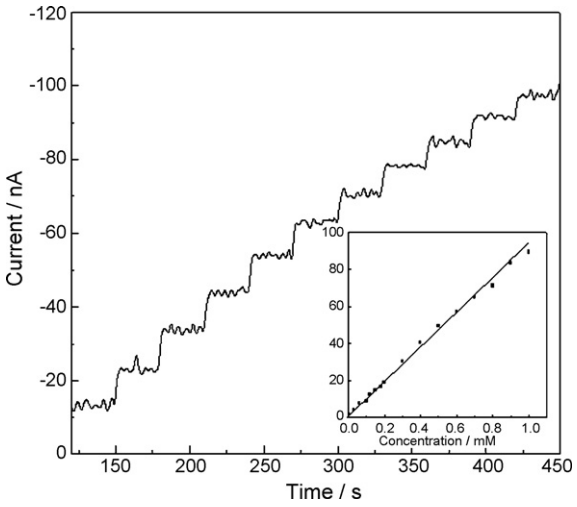


**Fig. 5.** Typical amperometric responses of the ZnO/cyt. *c* to successive additions of 100 μM $H_2O_2$ at applied potentials of 0.0 V (vs. Ag|AgCl) in 25 mM PBS (pH 7.2). Inset: calibration plot of steady-state currents against concentrations of $H_2O_2$.

and (B) 500 U $mL^{-1}$ catalase. The cathodic current increased gradually at ZnO/cyt. *c* surface (curve b) with the addition of PMA, which was reported to induce $H_2O_2$ production from the cells [43], and reduction current of ~1.8 nA was observed in 50 s, while no response was obtained at bare ZnO nanosheets film with the same addition of PMA (curve a). Interestingly, after injected 500 U $mL^{-1}$ catalase solution, a selective scavenger of $H_2O_2$, into the solution, the current shown in curve (b) decreased rapidly and went down to the almost background. Therefore, we can conclude that the generated increase of cathodic current at ZnO/cyt. *c* electrode located near the cells is ascribed to the enzymatic reduction of $H_2O_2$, which is effectively mediated by the cyt. *c* confined on the electrode. This observation substantially demonstrates the present developed third-generation $H_2O_2$ biosensor with nanostructured ZnO surface provides a model for reliable and durable determination of extracellular $H_2O_2$ and could be potentially useful for physiological and pathological investigations.

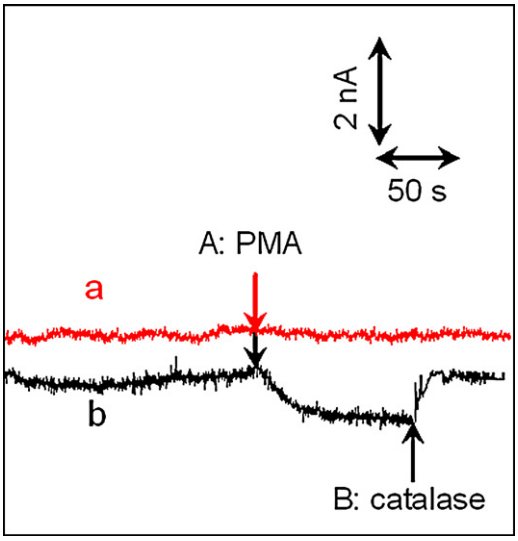


**Fig. 6.** Amperometric responses obtained at (a) ZnO nanosheets film and (b) ZnO/cyt. *c* electrode in 25 mM PBS (pH 7.2) containing 100 mM glucose at the applied potential of 0.0 V (vs. Ag|AgCl) with the addition of (A) 3 mM PMA and (B) 500 U $mL^{-1}$ catalase.

## 4. Conclusions

Direct and quasi-reversible electron transfer of cyt. *c* was developed at low-cost electrodeposited ZnO nanosheets with a formal potential of 338.2 mV (vs. Ag|AgCl). Cyt. *c* retained its intrinsic activity toward $H_2O_2$ after being confined on the nanostructured ZnO film. The enhanced electron transfer of cyt. *c* with positive redox formal potential, associated with the inherent catalytic activity of heme toward $H_2O_2$ prompted us to develop a $H_2O_2$ biosensor with high selectivity, free from the interferences of AA, DA, $NO_2^-$, and $O_2$. The remarkable analytical characteristics, together with the intrinsic biocompatibility of ZnO nanostructures sufficiently gave a basis for the detection of extracellular $H_2O_2$ released from human hepatoma cells. The present investigation provided a methodology to realize direct electron transfer between proteins and nanostructured semiconductors and on the basis of this platform to develop third-generation biosensors, as well as established a novel approach for the determination of extracellular $H_2O_2$, in which could be gained more understanding of the role that $H_2O_2$ and ROS plays in pathology and physiology.

## Acknowledgements

This work was financially supported by National Natural Science Foundation of China (20975075), the Program for New Century Excellent Talents in University (NCET-06-0380) and the Scientific Research Foundation for the Returned Overseas Chinese Scholars from State Education Ministry, China, and Nanometer Science Foundation of Shanghai (0952nm04900). Tongji University is greatly acknowledged.

## Appendix A. Supplementary data

Supplementary data associated with this article can be found, in the online version, at doi:10.1016/j.aca.2010.04.065.

## References

[1] M. Miah, T. Ohsaka, Anal. Chem. 78 (2006) 1200–1205.
[2] I.L. De Mattos, L. Gorton, T. Ruzgas, Biosens. Bioelectron. 18 (2003) 193–200.
[3] M.D.P.T. Sotomayor, A.A. Tanaka, L.T. Kubota, Electrochim. Acta 48 (2003) 855–865.
[4] T. Tatsuma, T. Ogawa, R. Sato, N. Oyama, J. Electroanal. Chem. 501 (2001) 180–185.
[5] R.E. Holt, T.M. Cotton, J. Am. Chem. Soc. 111 (1989) 2815–2821.
[6] M. Yang, F.L. Chung, M. Thompson, Anal. Chem. 65 (1993) 3713–3716.
[7] M.J. Eddows, H.A.O. Hill, J. Am. Chem. Soc. 101 (1979) 4461–4464.
[8] I. Taniguchi, M. Iseki, K. Toyosawa, I. Yamaguchi, K.J. Yasukouchi, Electroanal. Chem. 164 (1984) 385–391.
[9] J. Yu, H. Ju, Anal. Chem. 74 (2002) 3579–3583.
[10] L. Wang, E. Wang, Electrochem. Commun. 6 (2004) 49–54.
[11] X. Jiang, L. Shang, Y. Wang, S. Dong, Biomacromolecules 6 (2005) 3030–3036.
[12] H. Liu, Y. Tian, P. Xia, Langmuir 23 (2007) 9487–9494.
[13] L.A. Lyon, D.J. Pena, M.J. Natan, J. Phys. Chem. B 103 (1999) 5826–5831.
[14] K.R. Brown, D.G. Walter, M.J. Natan, Chem. Mater. 12 (2000) 306–313.
[15] D.L. Feldheim, K.C. Grabar, M.J. Natan, T.E. Mallouk, J. Am. Chem. Soc. 118 (1996) 7640–7641.
[16] H. Liu, Y. Tian, Z. Deng, Langmuir 23 (2007) 9487–9494.
[17] L. Mao, K. Yamamoto, Talanta 51 (2000) 187–195.
[18] L. Mao, P. Osborne, K. Yamamoto, T. Kato, Anal. Chem. 74 (2002) 3684–3689.
[19] S. Liu, Z. Dai, H. Chen, H. Ju, Biosens. Bioelectron. 19 (2004) 963–969.
[20] H. Yao, N. Li, S. Xu, J. Xu, J. Zhu, H. Chen, Biosens. Bioelectron. 21 (2005) 372–377.
[21] K. Lin, S. Chen, Biosens. Bioelectron. 21 (2006) 1737–1745.
[22] G. Shi, Z. Sun, M. Liu, L. Zhang, Y. Liu, Y. Qu, L. Jin, Anal. Chem. 79 (2007) 3581–3588.
[23] Z. Deng, Y. Gong, Y. Luo, Y. Tian, Biosens. Bioelectron. (2009) 2465–2469.
[24] S. Kar, B.N. Pal, S. Chaudhuri, D. Chakravorty, J. Phys. Chem. B 110 (2006) 4605–4611.
[25] S.Y. Bae, H.W. Seo, J. Park, J. Phys. Chem. B 108 (2004) 5206–5210.
[26] Z. Deng, Q. Rui, X. Yin, H. Liu, Y. Tian, Anal. Chem. 80 (2008) 5839–5846.
[27] J.J. Pankove, Optical Properties in Semiconductors, Prentice Hall, Englewood Cliffs, NJ, 1971.
[28] N.S. Pesika, K.J. Stebe, P.C. Searson, Adv. Mater. 15 (2003) 1289–1291.
[29] H.C. Ong, A.X.E. Zhu, G.T. Du, Appl. Phys. Lett. 80 (2002) 941–943.

[30] L.E. Brus, J. Phys. Chem. 90 (1986) 2555–2560.
[31] A.F. Nassar, W.S. Willis, J.F. Rusling, Anal. Chem. 67 (1995) 2386–2392.
[32] C. Wang, C. Yang, Y. Song, W. Gao, X. Xia, Adv. Funct. Mater. 15 (2005) 1267–1275.
[33] Y. Luo, H. Liu, Q. Rui, Y. Tian, Anal. Chem. 81 (2009) 3035–3041.
[34] Z. Deng, Y. Gong, Y. Luo, Y. Tian, Biosens. Bioelectron. 24 (2009) 2465.
[35] E. Topoglidis, Y. Astuti, F. Duriaux, M. Graetzel, J.R. Durrant, Langmuir 19 (2003) 6894.
[36] L. Zhu, D. Sun, T. Lu, C. Cai, C. Liu, W. Xing, Sci. China Ser. B: Chem. 50 (2007) 304.
[37] Z. Dai, S. Liu, H. Ju, Electrochim. Acta 49 (2004) 2139.
[38] X. Xu, B. Tian, J. Kong, S. Zhang, B. Liu, D. Zhao, Adv. Mater. 15 (2003) 1932.
[39] X. Zhang, J. Wang, W. Wu, S. Qian, Y. Man, Electrochem. Commun. 9 (2007) 2098–2104.
[40] Y. Liu, Y. Yang, H. Yang, Z. Liu, G. Shen, R. Yu, J. Inorg. Biochem. 99 (2005) 2046–2053.
[41] G. Zhao, J. Xu, H. Chen, Anal. Biochem. 350 (2006) 145–150.
[42] J. Liu, C. Guo, C. Li, Y. Li, Q. Chi, X. Huang, L. Liao, Ting Yu, Electrochem. Commun. 11 (2009) 202–205.
[43] Q. Lin, L. Jin, Z. Cao, Y. Lu, H. Xue, Y. Xu, Phytother. Res. 22 (2008) 740–745.